Interference of Surface Plasmon Waves and Plasmon Coupled Waveguide Modes for the Patterning of Thin Film

Yongjun Lim, Seyoon Kim, Hwi Kim, Jaehoon Jung, and Byoungho Lee, *Senior Member, IEEE*

***Abstract*—We analyze and propose a thin-film patterning method based on Kretschmann's attenuated total reflection (ATR) configuration where the surface plasmon mode and plasmon coupled waveguide modes coupled into a target photosensitive layer are generated. By analyzing stratified media with the help of extended transfer matrix method, we numerically visualize electromagnetic fields of surface plasmon waves and plasmon coupled waveguide modes. Through the interference of these modes, it is to be shown that our proposed configuration can be used in the optical lithography, especially for the thin-film patterning methods. Feasibility is tested by coating a dielectric layer on the gold layer in the ATR configuration.**

***Index Terms*—Optical lithography, plasmon coupled waveguide mode, surface plasmon resonance, thin-film patterning.**

I. Introduction

LOTS of methods related to the patterning of thin-films have been suggested, and it is recently shown that periodic patterns in thin-film can be formed by using surface plasmon polaritons [1], [2]. Moreover, following the scaling-down trend in the fabrication of the nano-scale devices, the research in optical lithography has been evolved and devoted to the renovation of the resolution limit [3]–[5]. Also, nanolithography utilizing the interference of surface plasmon waves has been recently proposed [6]–[12]. In these works, it is shown that using the surface bound wave generated by surface plasmons can make a certain interference pattern in the target photoresist (PR) layer when the incident p-polarized light passes through thin metallic masks, so the geometrical pattern formed by the interference of the surface plasmon waves can be inscribed on the photosensitive layer. However, according to the numerically calculated results shown in these papers, we can observe that the intensity distribution caused by the interference of surface plasmon resonance is mainly concentrated on the internal gap area of the metallic mask, and the fabrication of the metallic mask is required. Moreover, in fabricating periodic structures, it has already been shown that a near-field interference pattern can be formed by using a prism that can generate surface waves [13]. However, in this conventional prism configuration, it is not easy to increase the number of modes coupled into the target photosensitive layer and to effectively transfer the incident light into the target layer. In addition, it has already been shown that multiple resonance reflection dips can be formed by coating a dielectric layer on the surface of the thin gold film in the Kretschmann–Raether's attenuated total reflection (ATR) configuration [14], [15]. So, it was shown that the number of modes that can be coupled into the target layer can be controlled by varying the thickness and the refractive index of the dielectric layer coated on the gold layer. However, in those works, the surface plasmon mode propagating along the interface of the gold layer and the dielectric [polymethylmethacrylate (PMMA)] layer was not observed. In this paper, we will show the interference of the surface plasmon waves in our ATR device configuration and the interference of the waves propagating along the dielectric layer where the incident light wave can be efficiently coupled. Moreover, in our simulation results based on enhanced transfer matrix method (ETMM), we will show several interference patterns which can be generated by the interference irradiances of the surface plasmon mode and plasmon coupled waveguide modes. By visualizing the interference patterns, it becomes manifest to distinguish the surface plasmon mode from the plasmon coupled waveguide modes, and our proposed ATR configuration can be used for the patterning of the thin-film. We will organize this paper as follows. First, the dispersion relation in the metal-dielectric interface is to be briefly mentioned so that the basic mechanism of the generation and the interference of surface plasmon in the ATR configuration can be explained. Then, the generation of surface plasmon and plasmon coupled waveguide modes is experimentally demonstrated and numerically verified with the help of ETMM. Thereafter, the visualization of irradiances of interference patterns will be presented, and conclusions will be made finally.

Manuscript received July 8, 2007; revised October 8, 2007. This work was supported in part by the Creative Research Initiatives Program (Center for Active Plasmonics Application Systems) of the Ministry of Science and Technology of Korea and in part by the Korea Science and Engineering Foundation.

Y. Lim, S. Kim, H. Kim, and B. Lee are with the National Creative Research Center for Active Plasmonics Application Systems, Inter-University Semiconductor Research Center and School of Electrical Engineering, Seoul National University, Seoul 151-744, Korea (e-mail: byoungho@snu.ac.kr).

S. Kim was with the School of Electrical Engineering, Seoul National University, Seoul 151-744, Korea. He is now with the Agency for Defense Development of Korea, Daejeon 301-152, Korea.

J. Jung is with the School of Electrical, Electronics and Computer Engineering, Dankook University, Seoul 140-714, Korea.

Color versions of one or more of the figures in this paper are available online at http://ieeexplore.ieee.org.

Digital Object Identifier 10.1109/JQE.2007.912462

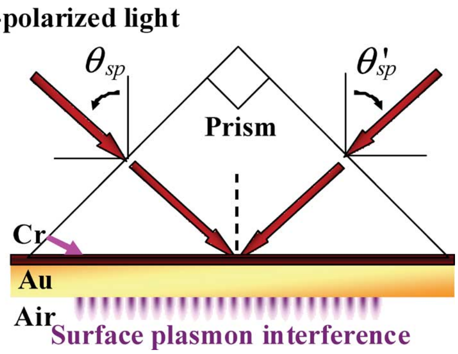

Fig. 1. Basic concept of the interference of surface plasmon waves.

II. Principles

A. Dispersion Relation

In the boundary between the dielectric layer and the metallic layer, there can occur collective electron oscillations when a p-polarized monochromatic wave satisfying a proper phase matching condition is incident at the boundary between semi-infinite metallic medium and dielectric medium [16]. This can be briefly explained by the following dispersion relation that can be found by solving Maxwell's equations and endowing them with proper boundary conditions. The resultant dispersion relation is given as

$$k_{\mathrm{sp}} = k_0 \sqrt{\frac{\varepsilon_d \cdot \varepsilon_m}{\varepsilon_d + \varepsilon_m}} \tag{1}$$

where k_{sp} and k_0 are, respectively, the wavenumbers of surface plasmon and the incident light, and ε_d and ε_m are, respectively, the electric permittivity of dielectric medium and metallic medium [17], [18]. This equation briefly explains that there is inherent phase mismatching in using an optical method for the excitation of the surface plasmon. So, a physical compensation should be added to the incident monochromatic p-polarized light. Usually, Kretschmann's ATR configuration is used to do so. For a specific incidence angle that exceeds the total internal reflection angle and satisfies the phase matching condition, the bulk of energy of the incident p-polarized light can be transferred into the interface of the metallic layer and the air due to the generation of the surface plasmon polariton. Due to the near-field enhancement caused by surface plasmon resonance at the interface of the metal and the dielectric, a highly intensive interference pattern generated by two evanescent waves counter-propagating toward each other along the interface can be made [1] as is shown in Fig. 1. If this interference pattern can be inscribed in photosensitive material, 1-D periodic structure can be efficiently formed in the photosensitive material layer. So, it is necessary that field distributions at the stratified media be analyzed and calculated to identify the characteristics of the light waves coupled into the target photosensitive layer. Thus, in Section II-B, the representation of electromagnetic (EM) field in layered media will be given.

B. Representation of Optical Fields in Layered Media Using ETMM

In this section, we briefly describe the ETMM [19]–[21] to visualize EM fields in our proposed ATR configuration. In 1-D multilayered structures, generally, the whole system can be decomposed into three regions, the entrance region, the inner region and the exit region. In the entrance region, the EM field for a p-polarized light can be given as follows:

$$E_{x,I} = \frac{k_{z,I}}{n_I k_0}\left[1 \cdot \exp(jk_{z,I}z) + R \cdot \exp(-jk_{z,I}z)\right]\exp(jk_x x) \tag{2}$$

$$E_{z,I} = \frac{k_x}{n_I k_0}\left[-1 \cdot \exp(jk_{z,I}z) + R \cdot \exp(-jk_{z,I}z)\right]\exp(jk_x x) \tag{3}$$

$$\begin{aligned} H_{y,I} &= \frac{1}{j\omega\mu_0}(\partial_z E_x - \partial_x E_z) \\ &= \frac{n_I k_0}{\omega\mu_0}\left[1 \cdot \exp(jk_{z,I}z) - R \cdot \exp(-jk_{z,I}z)\right]\exp(jk_x x) \end{aligned} \tag{4}$$

where $E_{m,n}$, $H_{m,n}$, k_0 and $k_{m,n}$ are, respectively, the electric field, the magnetic field, the wavevector in vacuum and the wavevector along the $m(= x, y, z)$ direction in the nth region. R and T are, respectively, reflectance and transmittance. In the internal ith region of the stratified medium, the EM field can be represented as follows:

$$E_{x,i} = \frac{k_{z,i}}{n_i k_0}\left\{a_i \exp\left[jk_{z,i}(z - l_{i-1})\right] + b_i \exp\left[-jk_{z,i}(z - l_i)\right]\right\} \tag{5}$$

$$E_{z,i} = \frac{k_x}{n_i k_0}\left\{-a_i \exp\left[jk_{z,i}(z - l_{i-1})\right] + b_i \exp\left[-jk_{z,i}(z - l_i)\right]\right\} \tag{6}$$

$$H_{y,i} = \frac{n_i k_0}{\omega\mu_0}\left\{a_i \exp\left[jk_{z,i}(z - l_{i-1})\right] - b_i \exp\left[-jk_{z,i}(z - l_i)\right]\right\} \tag{7}$$

where a_i and b_i are, respectively, complex amplitudes for forward and backward waves in the ith region. l_i is the total distance of the internal region, and n_i and ω are, respectively, the refractive index at the ith region and the frequency of the incident light. In the exit region, the EM field for the p-polarized light can be given as follows:

$$E_{x,f} = \frac{k_{z,f}}{n_f k_0} T \exp\left[jk_{z,f}(z - l_N)\right] \tag{8}$$

$$E_{z,f} = -\frac{k_x}{n_f k_0} T \exp\left[jk_{z,f}(z - l_N)\right] \tag{9}$$

$$H_{y,f} = \frac{n_f k_0}{\omega\mu_0} T \exp\left[jk_{z,f}(z - l_N)\right]. \tag{10}$$

After considering boundary conditions between the adjacent layers, the resultant equations can be given. Hence, the continuity of E_x and H_y should be maintained to satisfy the phase matching condition. Moreover, in calculating field intensity distribution and finding the value of the wave vectors in each

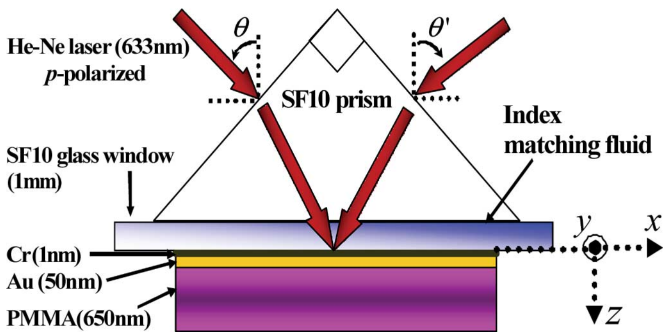

Fig. 2. Schematic diagram of our proposed ATR device.

layer, the final matrix representation with respect to E_x and H_y can be arranged as

$$\begin{pmatrix} \frac{k_{z,I}}{n_I} & \frac{k_{z,I}}{n_I} \\ n_I & -n_I \end{pmatrix} \begin{pmatrix} 1 \\ R \end{pmatrix} = \left[\prod_{i=1}^{N} \begin{pmatrix} \frac{k_{z,i}}{n_i} & \frac{k_{z,i}}{n_i} X_i \\ n_i & -n_i X_i \end{pmatrix} \times \begin{pmatrix} \frac{k_{z,i}}{n_i} X_i & \frac{k_{z,i}}{n_i} \\ n_i X_i & -n_i \end{pmatrix}^{-1} \right] \begin{pmatrix} \frac{k_{z,f}}{n_f} \\ n_f \end{pmatrix} T \quad (11)$$

where X_i is a phase term at the ith layer. Using this resultant representation enables us to find reflectance in 1-D multilayered structure, and the reflectance can be calculated by $R \cdot R^*$, where R^* indicates the complex conjugation of the reflectance, R. In addition, the EM field intensity can be calculated and visualized. In our simulation method, to solve the diverging problem caused by the phase term X_i, we directly refer to the stabilization method described in [21]. By using this ETMM, we can numerically determine whether the incident light exceeding the critical angle is coupled into the dielectric layer or into the interface of the metallic layer and the dielectric layer.

C. Experimental Demonstration of the Generation of Multiple Reflection Dips

In our ATR device, the configuration is composed of SF10 prism, SF10 glass window, 1-nm Cr layer, 50-nm Au layer and a dielectric layer, and index matching fluid is used between the prism and the glass window as shown in Fig. 2. After looking for an appropriate thickness of the dielectric layer, the comparison of the measured reflectance with the simulation result is shown in Fig. 3. Here, PMMA is selected for the dielectric material to be coated, and the thickness of the PMMA layer through the calculation is 650 nm. Here, the thickness of the Au layer and that of the PMMA layer are optimized by using the ETMM so that the incident light can be wholly coupled into the target dielectric layer. In our numerical simulation, the used refractive indexes of SF10, Cr, Au and PMMA at the wavelength of 633 nm are, respectively, 1.73, 3.14+i3.32, 0.20+i3.32 and 1.46 [22], [23]. In Fig. 4, the experimental results for the measurement of the reflectance (for 633-nm wavelength) in the Kretchmann's ATR configuration are shown together. In Fig. 4, the curve that has no reflection dip shows the reflectance of the SF 10 prism without any metallic layers and the PMMA layer. This curve helps us prove that resonant angles related to surface plasmon mode and

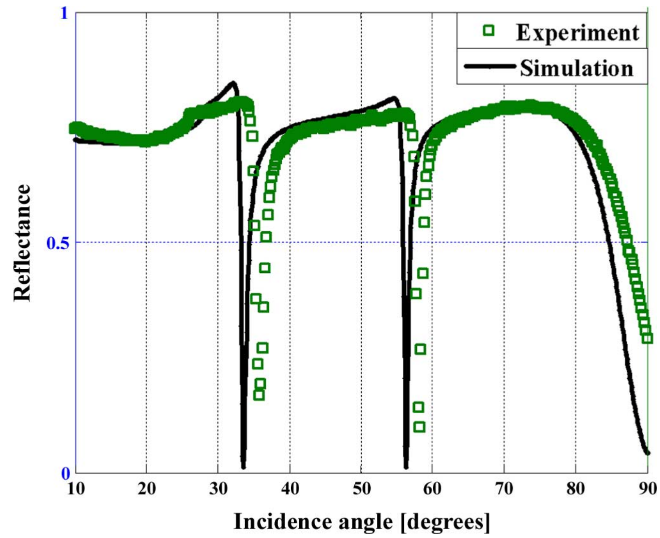

Fig. 3. Comparison of the experimental result (normalized value) and the simulation result.

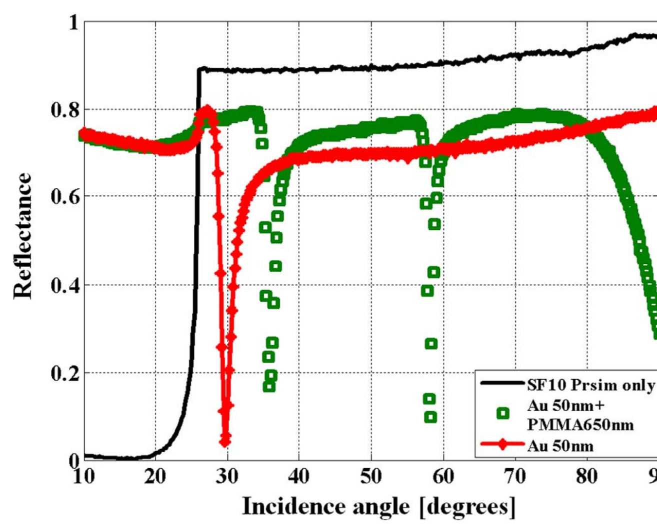

Fig. 4. Measurement of reflectance (normalized value).

plasmon coupled waveguide modes occur when they excess the critical angle. Also, in this figure, the curve that has one reflection dip is the measurement of reflectance of the ATR device configuration, and the reflectance curve that has three dips is that of the optimized PMMA layer added to the original ATR configuration. As is shown in Fig. 4, we can observe that the incident p-polarized light is absorbed in the ATR device configuration. So, by calculating and visualizing field distributions at these reflection dips with the help of the ETMM described through (2)–(11), into which region the incident light is coupled can be analyzed. Also, the calculation of the wave vector component in the region where the incident light is transferred can make the difference between the surface-bound wave (surface plasmon mode) and the propagating wave (plasmon coupled waveguide mode). Moreover, we can observe that the incident monochromatic light can be effectively coupled into the PMMA layer as is seen in Fig. 4. The measured resonance angle θ_{sp} for the basic ATR configuration, composed of SF10 prism, 1-nm

Cr layer and 50-nm Au layer, was 29.8° as shown in Fig. 4. In the measured reflectance curve possessing three reflectance dips for the PMMA-added configuration, the three resonance angles were $\theta_A = 35.8°$, $\theta_B = 58.2°$, and $\theta_C = 90°$. When the incidence angle is adjusted to these three angles, the incident light can be absorbed in the ATR configuration. Here, it is necessary to explain the absorption of the incident light in our proposed configuration. On the one hand, this can be explained by calculating the field distribution and the corresponding wave vector component in each layer at those resonant angles. By using our ETMM, the EM field distributions, such as the electric field E_x, the magnetic field H_y and the electric flux density D_z, can be analyzed. On the other hand, the characteristic of the coupled light can be demonstrated by making the coupled light interfere with its counter propagating waves at resonant angles. By visualizing the interference patterns, it can be concluded that waveguide modes do exist along the PMMA layer under the resonance condition. These modes can be regarded as plasmon coupled waveguide modes because they are generated by the incident p-polarized light satisfying the specific resonance angles [14], [15]. At these specific angles, the incident p-polarized light excites eigenmodes of the Au–PMMA composite waveguide through side-illumination and phase-matching. Then, the multiple reflectance dips shown in Fig. 3 are originated from the lossy property of the eigenmodes. In Section III, by visualizing the interference patterns at those resonance angles, the characteristics of the coupled light in the PMMA layer is to be estimated so that our proposed ATR configuration can be used for the patterning of thin-films. Also, we can see different behavior of the coupled light at each resonance angle of our PMMA-added ATR configuration.

D. Practical Implementation of the Proposed Thin-Film Patterning Method

So far, we have tested the feasibility of the thin-film patterning method in the visible frequency region by using the wavelength of 633 nm, and we chose PMMA as the dielectric material because it is easy to control its thickness by changing the revolutions-per-minute (rpm) speed of the spin-coater. However, PMMA is not absorptive in this excitation wavelength, 633 nm, and it is generally used as a high resolution resist which requires higher frequency sources such as extreme UV and deep UV, or e-beam. Hence, the practical wavelengths, for which PMMA can be used as a photosensitive material and the corresponding PMMA-added ATR configuration can be implemented, are 193, 248, and 308 nm [3], [24]. Also, for these wavelengths, instead of gold, aluminum is used as the metallic layer. More specifically, for example, at the wavelength of 248 nm, the modified configuration can be composed of sapphire prism, aluminum with the thickness of 19 nm and PMMA with the thickness of 200 nm, and their refractive indexes are, respectively, 1.84, 0.19+i2.94 and 1.49. By using these materials and by adopting these parameters, our proposed configuration shown in the Section II-C can be applicable practically for the thin-film patterning method.

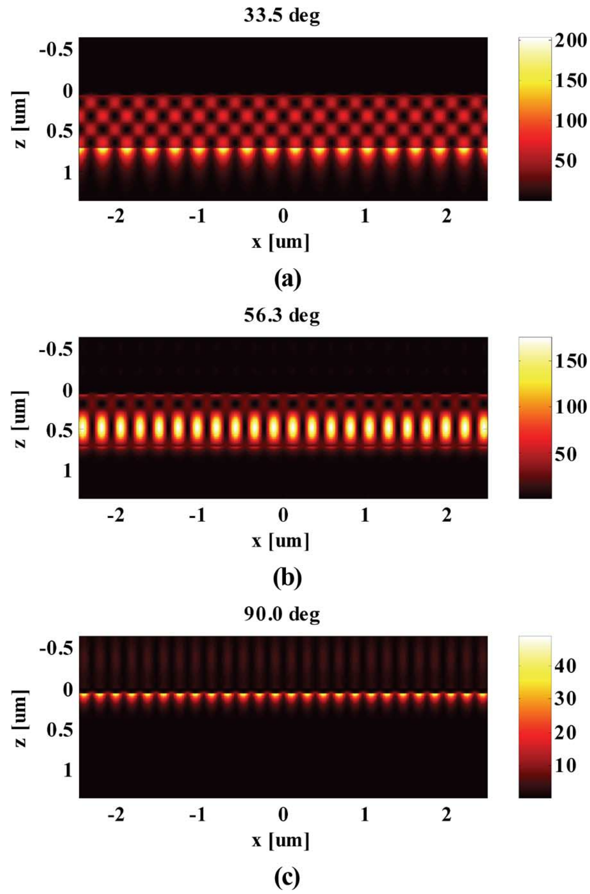

Fig. 5. Interference patterns for the structure of Fig. 2. (a) Visualization of I_{θ_A}. (b) Visualization of I_{θ_B}. (c) Visualization of I_{θ_C}.

III. Visualization of the Interference of the Optical Fields

In this section, the numerically calculated intensity distribution generated by the interference of surface plasmon waves and plasmon coupled waveguide modes is to be shown. In the previous section, we experimentally demonstrated the occurrence of resonant reflection dips in our proposed ATR configuration. In our experiment and the corresponding numerical analysis with ETMM, three resonance angles were found, and the characteristics of the coupled light wave in each layer can be described by visualizing the intensity of each interference pattern. We obtained those resonant angles as $\theta_A(= 35.8°)$, $\theta_B(= 58.2°)$ and $\theta_C(= 90°)$ in the experimental result. However, the corresponding simulation results for the three resonant angles are $\theta_A(= 33.5°)$, $\theta_B(= 56.3°)$ and $\theta_C(= 90°)$ as shown in Fig. 3. So, for the convenience of the numerical calculation, we follow these numerically calculated resonance angles. The intensity distribution can be given as follows:

$$I_{\theta_i} = \left|E_{x,\theta_i} + E_{x,\theta_i'}\right|^2 + \left|E_{z,\theta_i} + E_{z,\theta_i'}\right|^2 \quad i = A, B, C \tag{12}$$

where the angle convention of θ_i and θ_i' is shown in Fig. 2, and θ_i and θ_i' are considered to have equal values. In Fig. 5, we can observe that the incident p-polarized light is coupled into the PMMA layer [Fig. 5(a) and (b)] and the interface in the Au layer and the PMMA layer [Fig. 5(c)] at the corresponding resonance

TABLE I
CALCULATED WAVE NUMBERS (NORMALIZED WITH RESPECT TO k_0) AND THE PERIOD OF FRINGES IN EACH LAYER AT EACH RESONANT ANGLE

Resonant angle	Layer	k_x/k_0	k_z/k_0	Period of fringes
33.5°	Cr	1.0746	3.0545+3.4129i	294.5nm
	Au		0.1903+3.4890i	
	PMMA		0.9883	
56.3°	Cr	1.3539	3.0057+3.4684i	233.8nm
	Au		0.1852+3.5847i	
	PMMA		0.5464	
90°	Cr	1.6194	2.9500+3.5338i	195.4nm
	Au		0.1798+3.6929i	
	PMMA		0.7006i	

angles. Here, in Fig. 5, the origin ($z = 0$) of the coordinates is located at the chromium-SF10 glass interface (see Fig. 2). In Fig. 5(a), the intensity distribution of the interference pattern is relatively high at the interface of the PMMA and the air. In this case, the coupled light is not only guided along the PMMA layer but also along the interface of the PMMA layer and the air. The evanescent field is formed along the interface of the PMMA layer and the air, which is similar to the case shown in Fig. 5(c). However, by calculating wavenumbers in each layer, we can discriminate the characteristics of the coupled light at each resonance angle. In Fig. 5(b), the incident light is entirely coupled into the PMMA layer, so this can be regarded as plasmon coupled waveguide modes. In Fig. 5(c), the interference pattern is generated at the interface of the Au layer and the PMMA layer, so this interference pattern is induced by surface plasmon resonance. Also, these explanations can be demonstrated by the calculation of the wavenumber in each layer, which is shown in Table I. From the calculated wavenumbers, the coupled lights at the angles $\theta_A(= 33.5°)$ and $\theta_B(= 56.3°)$ are regarded as guiding modes, i.e, plasmon coupled waveguide modes, where the calculated wavenumbers in the PMMA layer are real, and the coupled light at the angle $\theta_C(= 90°)$ is a surface-bound wave, i.e., surface plasmon mode, where one of the calculated wavenumbers in the PMMA layer takes the imaginary value. Additionally, as shown in Fig. 5, the field intensity of the interference is considerably high. This property will help us fabricate 1-D periodic structure in the target photosensitive layer. Moreover, from the viewpoints of utilizing optical power efficiency, this is one of the most significant advantages in using our proposed methods when our proposed configuration is used in the field of optical lithography. When multiple beam paths coupled into the PMMA layer are generated, various interference patterns can be made. So, the combination of the resultant interference patterns shown in Fig. 5 can be made, and the schematic diagram for this method is shown in Fig. 6(a). In Fig. 6(b)–(d), the possible combinations of two different cases chosen from three kinds of the interference patterns in Fig. 5 are shown in Fig. 6(b)–(d). In Fig. 6(b)–(d), the ratio of irradiance to each other is set to be equal. Especially, as shown in Fig. 6(d), we can observe an interference pattern possessing a surface periodic structure and an internal periodic structure in one layer. When the dielectric material sensitive to the wavelength of 633 nm is used, it will be possible to fabricate that periodic structure. Furthermore, we can expect that changing intensity ratio at the resonance-pair angles makes it possible for us to fabricate various patterns in the dielectric layer coated on the metallic layer in the ATR configuration without fabricating masks used in conventional optical lithography.

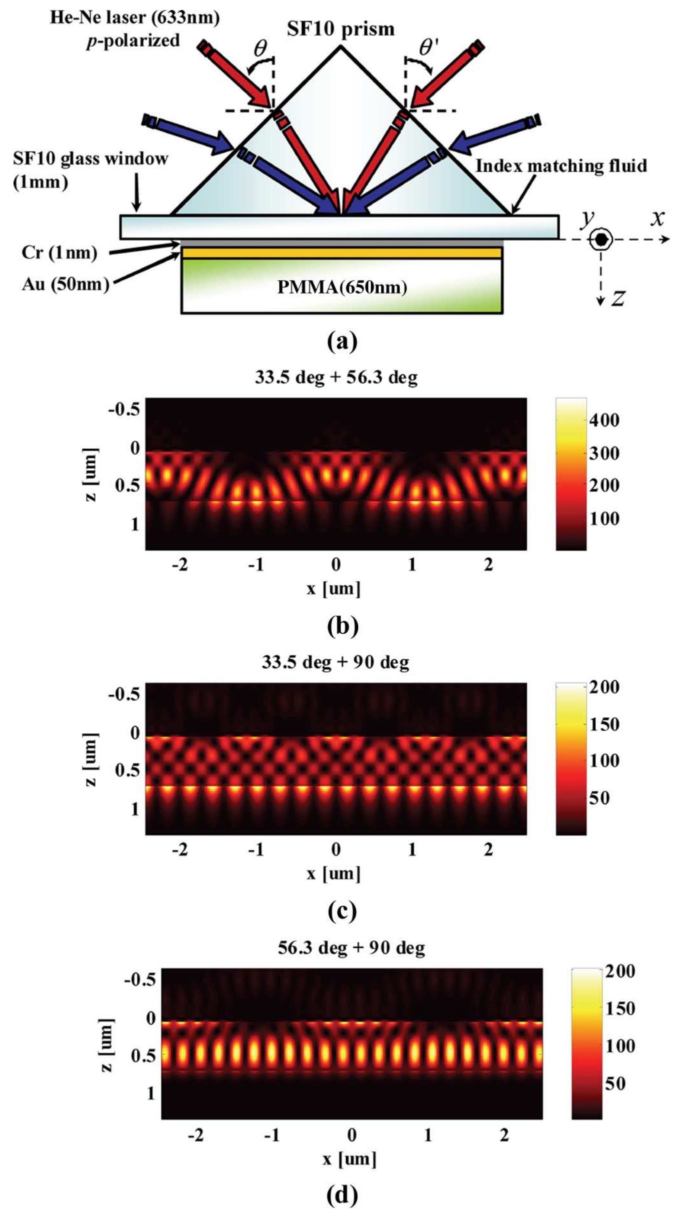

Fig. 6. (a) Schematic diagram of the interference patterns generated at two different resonance-pair angles. (b) Combined irradiance pattern of Fig. 5(a) and (b). (c) Combined irradiance pattern of Fig. 5(a) and (c). (d) Combined irradiance pattern of Fig. 5(b) and (c).

IV. Conclusion

In this paper, the method for the patterning of thin-films, based on the interference of the highly confined modes generated by surface plasmon resonance and by plasmon coupled waveguide modes, has been proposed. By finding the ATR configuration with the surface plasmon mode and plasmon coupled waveguide modes that can be formed into the target dielectric layer, we numerically analyzed various kinds of interference patterns that can be simply made in the ATR structure. In addition, according to the numerically visualized results based on ETMM, we clarified the surface plasmon mode and plasmon coupled waveguide modes. Furthermore, by visualizing the interference of the generated surface plasmon mode and waveguide modes in the PMMA layer, we suggested an optical lithography method that can form two different grating structures in the single thin-film layer.

References

[1] L. Röntzsch, K.-H. Heinig, J. A. Schuller, and M. L. Brongersma, "Thin film patterning by surface-plasmon-induced thermocapillarity," *Appl. Phys. Lett.*, vol. 90, 2007, art. 044105.

[2] X. Guo, J. Du, Y. Guo, and J. Yao, "Large-area surface-plasmon polariton interference lithography," *Opt. Lett.*, vol. 31, no. 17, pp. 2613–2615, 2006.

[3] M. Rothschild, T. M. Bloomstein, T. H. Fedynyshyn, R. R. Kunz, V. Liberman, M. Switkes, N. N. Efremow, Jr., S. T. Palmacci, J. H. C. Sedlacek, D. E. Hardy, and A. Grenville, "Recent trends in optical lithography," *Lincoln Lab. J.*, vol. 14, pp. 221–236, 2003.

[4] S. Okaaki, "Resolution limits of optical lithography," *J. Vac. Sci. Technol. B*, vol. 9, pp. 2829–2833, 1991.

[5] T. A. Brunner, "Why optical lithography will live forever," *J. Vac. Sci. Technol. B*, vol. 21, pp. 2532–2537, 2003.

[6] W. Srituravanich, N. Fang, C. Sun, Q. Luo, and X. Zhang, "Plasmonic nanolithography," *Nano Lett.*, vol. 4, pp. 1085–1088, 2004.

[7] W. Srituravanich, S. Durant, H. Lee, C. Sun, and X. Zhang, "Deep subwavelength nanolithography using surface plasmon modes on planar silver mask," *J. Vac. Sci. Technol. B*, vol. 23, pp. 2536–2539, 2005.

[8] Z.-W. Liu, Q.-H. Wei, and X. Zhang, "Surface plasmon interference nanolithogrphy," *Nano Lett.*, vol. 5, pp. 957–961, 2005.

[9] X. Luo and T. Ishihara, "Subwavelength photolithography based on surface-plasmon polariton resonance," *Opt. Exp.*, vol. 12, pp. 3055–3065, 2004.

[10] X. Luo and T. Ishihara, "Surface plasmon resonant interference nanolithography technique," *Appl. Phys. Lett.*, vol. 84, pp. 4780–4782, 2004.

[11] D. B. Shao and S. C. Chen, "Numerical simulation of surface-plasmon-assisted nanolithography," *Opt. Exp.*, vol. 13, pp. 6964–6973, 2005.

[12] D. B. Shao and S. C. Chen, "Surface-plasmon-assisted nanoscale photolithography by polarized light," *Appl. Phys. Lett.*, vol. 86, 2005, article 253107.

[13] J. Teteris and M. Reinfelde, "Subwavelength-period gratings in amorphous chalcogenide thin-films," *J. Opt. A: Pure Appl. Opt.*, vol. 6, pp. S151–S154, 2004.

[14] K. Choi, H. Kim, Y. Lim, S. Kim, and B. Lee, "Analytic design and visualization of multiple surface plasmon resonance excitation using angular spectrum decomposition for a Gaussian input beam," *Opt. Exp.*, vol. 13, pp. 8866–8874, 2005.

[15] G. P. Wang, T. Sugirua, and S. Kawata, "Holography with surface-plasmon-coupled waveguide modes," *Appl. Opt.*, vol. 40, pp. 3649–3653, 2001.

[16] H. Raether, *Surface Plasmons on Smooth and Rough Surfaces and on Gratings*. Berlin, Germany: Springer-Verlag, 1988.

[17] W. L. Barnes, A. Dereux, and T. W. Ebbesen, "Surface plasmon subwavelength optics," *Nature*, vol. 424, pp. 824–830, 2003.

[18] A. V. Zayats, I. I. Smolyaninov, and A. A. Maradudin, "Nano-optics of surface plasmon polaritons," *Phys. Reports*, vol. 408, pp. 131–314, 2005.

[19] B. E. A. Saleh and M. C. Teich, *Fundamentals of Photonics*, 2nd ed. New York: Wile, 2007.

[20] M. Born and E. Wolf, *Principles of Optics: Electromagnetic Theory of Propagation, Interference and Diffraction of Light*, 7th ed. Cambridge, U.K.: Cambridge Univ. Press, 1999.

[21] M. G. Moharam, D. A. Pommet, E. B. Grann, and T. K. Gaylord, "Stable implementation of the rigorous coupled-wave analysis for surface-relief gratings: Enhanced transmittance matrix approach," *J. Opt. Soc. Amer. A*, vol. 12, pp. 1077–1086, 1995.

[22] P. B. Johnson and R. W. Christy, "Optical constants of transition metals: Ti, V, Cr, Mn, Fe, Co, Ni, and Pd," *Phys. Rev. B*, vol. 9, pp. 5056–5070, 1974.

[23] *"Handbook of Optical Constants of Solids,"* E. D. Palik, Ed., Academic, New York, 1985.

[24] C. Wochnowski, M. A. S. Eldin, and S. Metev, "UV-laser-assisted degradation of poly(methyl methacrylate)," *Polymer Degrad. Stabil.*, vol. 89, pp. 252–264, 2005.

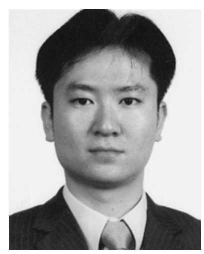

Yongjun Lim received the M.S. degree from the School of Electrical Engineering, Seoul National University, Seoul, Korea, in 2006, where he is currently pursuing the Ph.D. degree.

His main research interest is surface plasmon sensors and applications.

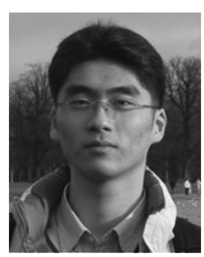

Seyoon Kim received the M.S. degree from the School of Electrical Engineering, Seoul National University, Seoul, Korea, in 2007.

He is currently with the Agency for Defense Development of Korea.

Hwi Kim received the Ph.D. degree from the School of Electrical Engineering, Seoul National University, Seoul, Korea, in August 2007.

He is currently a Postdoctoral Researcher in the National Creative Research Center for Active Plasmonics Application Systems, Seoul National University. He has authored or co-authored about 30 journal papers in the field of diffractive optical field simulation for nano-structures and holographic devices.

Jaehoon Jung received the Ph.D. degree from School of Electrical Engineering, Seoul National University, Seoul, Korea, in 2000.

After working for Samsung Electronics for four years, he moved to Dankook University, Seoul, Korea, where he is currently an Assistant Professor. His main interests are surface plasmon resonance sensors and waveguide devices.

Byoungho Lee received the Ph.D. degree in electrical engineering and computer science from the University of California at Berkeley in 1993.

In 1994, he joined the faculty of the School of Electrical Engineering, Seoul National University, where he is now a Full Professor. He has published more than 200 international journal papers and more than 320 international conference papers including 45 invited papers. His recent research interests are diffractive optics for nano-structures and surface plasmon polaritons. He is currently the Director of the National Creative Research Center for Active Plasmonics Application Systems funded by the Ministry of Science and Technology of Korea.

Dr. Lee is currently an Associate (Topical) Editor of *Applied Optics, Optical Fiber Technology*, and *Journal of the Society for Information Display*. He has also served as an Oversea Editor for *Japanese Journal of Applied Physics*. He is a fellow of the Optical Society of America and a fellow of the SPIE.